Study of Corotating Interaction Regions in the Ascending Phase of the Solar Cycle: Multi-spacecraft Observations

J. A. Gonzalez-Esparza, E. Romero-Hernandez & P. Riley

Solar Physics
A Journal for Solar and Solar-Stellar Research and the Study of Solar Terrestrial Physics

ISSN 0038-0938
Volume 285
Combined 1-2

Sol Phys (2013) 285:201-216
DOI 10.1007/s11207-013-0282-z

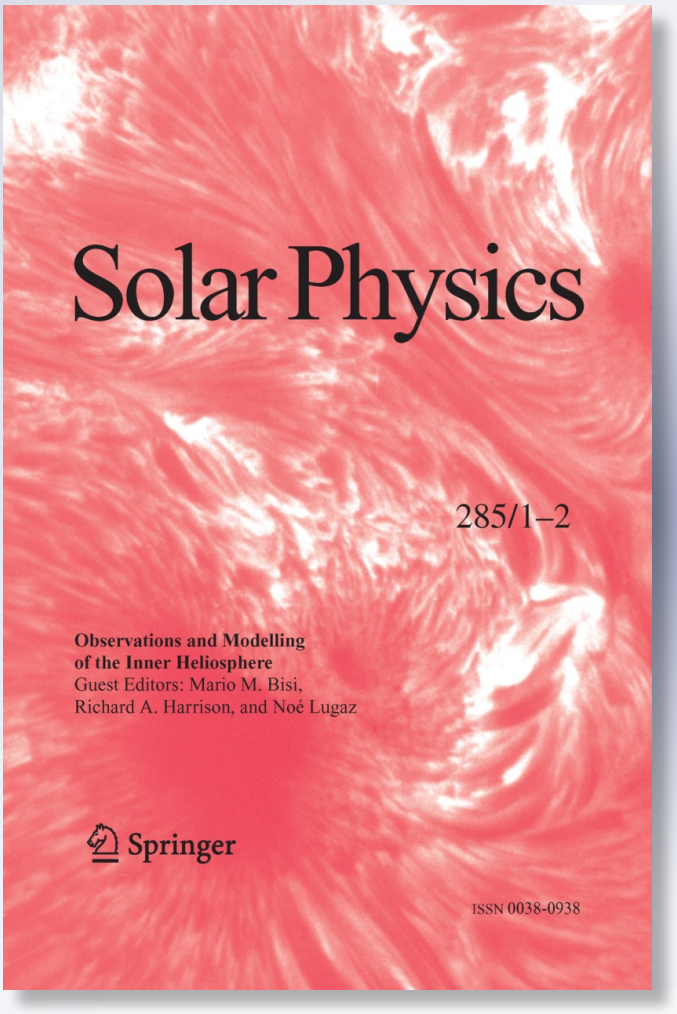

Springer

Solar Phys (2013) 285:201–216
DOI 10.1007/s11207-013-0282-z

Study of Corotating Interaction Regions in the Ascending Phase of the Solar Cycle: Multi-spacecraft Observations

J.A. Gonzalez-Esparza · E. Romero-Hernandez · P. Riley

Received: 26 March 2012 / Accepted: 21 March 2013 / Published online: 12 April 2013

Abstract We combined simultaneous solar wind observations from five different spacecraft: *Helios 1*, *Helios 2*, IMP-8, *Voyager 1* and *Voyager 2*, from November 1977 to February 1978 (Carrington rotations 1661 – 1664, ascending phase of Solar Cycle 21). The concurrence of the five trajectories makes this interval unique for the purpose of studying solar wind dynamics during this phase of the cycle. We analyzed the observations identifying five corotating interaction regions (CIRs) and produced maps of interplanetary large-scale features, unifying and summarizing the data. The maps show the compressive events and the magnetic sectors associated with the solar wind streams causing the CIRs. We analyzed the relative position of the stream interfaces immersed within the CIRs. About 70 % of the stream interfaces in this study were located closer to the forward edge of the CIR. From the analysis of the geometry of the stream interfaces, we found that all the CIRs presented latitudinal tilts, having their fronts pointing towards the ecliptic plane and their tails northwards or southwards. These results are in agreement with the origin of the fast streams coming from mid-latitude coronal holes and the predominance of forward shocks over reverse shocks bounding the CIRs, which characterize this phase of the cycle. From the analysis of the ratio of dynamic pressures between fast and slow solar wind streams associated with the CIRs, we found that in about 60 % of the cases the fast stream was transferring momentum to the slow one ahead, but in the rest of the cases the momentum was flowing sunward. This result indicates significant inhomogeneities in the solar wind streams during the ascending

Observations and Modelling of the Inner Heliosphere
Guest Editors: Mario M. Bisi, Richard A. Harrison, and Noé Lugaz

J.A. Gonzalez-Esparza (✉) · E. Romero-Hernandez
MEXART, Inst. de Geofisica, Unidad Michoacan, Universidad Nacional Autonoma de Mexico, antigua carretera a Patzcuaro # 8701 Ex-Hda. San Jose de la Huerta, Morelia, Michoacan 58089, Mexico
e-mail: americo@geofisica.unam.mx

E. Romero-Hernandez
Posg. Ciencias de la Tierra, Universidad Nacional Autonoma de Mexico, Ciudad Universitaria, Mexico DF 04510, Mexico

P. Riley
Predictive Science, Inc., 9990 Mesa Rim Road, San Diego, CA, USA

phase of the cycle that affect the local form and evolution of CIR events. We did a limited comparison between a global magneto-hydrodynamic (MHD) model of SW flows and the orientation of the SI from *in-situ* observations, we found, in general, a qualitative agreement between the pressure profiles at 1 AU predicted by the model and the inclinations of the stream interfaces deduced from the data analysis.

Keywords Corotating interaction regions · Solar wind dynamics · Interplanetary physics · Stream interfaces · Inner heliosphere

1. Introduction

Corotating interaction regions (CIRs) are large-scale interplanetary (IP) structures produced by the interaction of fast solar wind (SW) overtaking slow SW driven by the rotation of the Sun. When fast SW catches slow SW, a compression region, bound by forward (F) and reverse (R) waves, forms. As the regions evolve with distance from the Sun, they increase in size and their compression waves steepen into shocks. CIRs play a fundamental role in the large-scale dynamics of the SW and their evolution and interactions cause global changes in the heliosphere. Some authors prefer the term stream interaction regions (SIRs) for those events associated with short lived fast streams producing interaction regions that do not last for more than one solar rotation, as in general occurs during the ascending phase of the solar cycle. Their lack of recurrence from one rotation to the next led them to use the term SIRs, rather than CIRs; however, for simplicity, we will retain the latter term.

In this study, we combine simultaneous in-ecliptic observations from five spacecraft: *Helios 1* (H1), *Helios 2* (H2), IMP-8 (IMP), *Voyager 1* (V1) and *Voyager 2* (V2), during the ascending phase of Solar Cycle 21, to analyze characteristics and geometries of CIRs around 1 AU. The interval covered by this study goes from November 1977 to March 1978 (Carrington rotations 1661 – 1664), corresponding to the early stage of the *Voyager* mission. We chose this interval because the angular separations between the five in-ecliptic spacecraft were less than 60° in longitude and the *Voyagers* were not yet too far away from Earth. This conjunction of the five trajectories, confined into a limited range of longitudes and heliocentric distances, make this interval unique for the purposes of studying CIR evolution.

Burlaga *et al.* (1980) studied this multi-spacecraft data set in the period 22 November to 6 December 1977, and identified three types of IP flow detected by the five missions. They combined a large set of data including plasma, magnetic field, plasma waves, and energetic protons, to discuss the characteristics of three events: a stream interface (SI) immersed within a CIR, a transient shock associated with a solar flare, and a transient shock followed by a CME. González-Esparza and Smith (1996) compared CIR in-ecliptic observations detected by *Pioneer 10* and *11* (declining phase of Cycle 20), *Voyager 1* and *2* (ascending phase of Cycle 21), and *Ulysses* (post maximum of Cycle 22) from 1 to 5 AU. They found that in about half of the CIRs the dynamic pressure of the slow SW was higher than the one of the fast SW, implying that for those CIRs the slow SW transferred momentum to the fast SW. González-Esparza (1999) studied the geometry of this combined set of in-ecliptic CIRs, finding variations in the orientation of the SI associated with the CIRs: the SIs detected by *Ulysses* were oriented nearly perpendicular to the ecliptic plane, whereas the ones detected by the other missions (*Voyager 1* and *2*, and *Pioneer 11*) presented significant tilts with respect to the ecliptic plane (pointing towards southern or northern heliolatitudes).

Ulysses out-of-ecliptic observations increased our interest in the three-dimensional heliosphere structure. One of the main results obtained by *Ulysses* after the Jupiter flyby (descending phase of Solar Cycle 22) was the absence, from about 28° to 38° south latitude, of

F shocks leading CIRs and the continuous presence of R shocks trailing these CIRs (Gosling *et al.*, 1993; Pizzo and Gosling, 1994; Balogh *et al.*, 1995; González-Esparza *et al.*, 1996). On the basis of the strong latitudinal shear flows of SW velocity inside these CIRs and the predictions by the three-dimensional model of corotating flows (Pizzo, 1991) Gosling *et al.* (1993) suggested that this phenomenon, discovered by Ulysses observations at mid-latitudes, could be explained if the CIRs were tilted with respect to the solar rotation axis. This tilt geometry causes the front of the CIR to evolve more strongly at low latitudes (close to the ecliptic plane) while the trailing edge evolves more strongly at higher latitudes and produces a strong latitudinal shear flow inside the interaction region (see *e.g.*, Figure 10 in Riley *et al.*, 2012b). Riley *et al.* (1996) studied the orientations of the F and R shocks bounding these CIRs detected by *Ulysses*, finding that shock strength appeared to be modulated by the tilt of the solar dipole, peaking at latitudes roughly equivalent to the maximum extent of the heliospheric current sheet (HCS). Additionally, they found that F shocks propagated equatorward and westward, while R shocks propagated poleward and eastward, suggesting that these CIRs were systematically tilted in the heliosphere.

A characteristic signature of a CIR is the SI embedded within it, which is a boundary separating fast and slow compressed SW flows. Fast and slow streams carry different magnetic fields and cannot be mixed; there is no net flow across the SI. This boundary is distinguished by an abrupt drop in density and a similar increase in temperature and is associated with a high pressure region (Burlaga, 1974). A SI in the inner heliosphere is bound by an interaction region, which gradually expands in the outer heliosphere (Figure 2 in Siscoe, 1976). Siscoe and Finley (1969) predicted east–west and north–south deflections of SW velocity around SIs. These deflections result from the orientation of the SI and the high thermal and magnetic pressures associated with the interface (see *e.g.*, Figure 1 in Riley *et al.*, 2012b). Gosling *et al.* (1978) studied 23 SIs detected by IMP 6, 7, and 8 at 1 AU between 1971 and 1974. They produced a superposed epoch analysis to emphasize the overall structure of the SIs and reported that: i) the behavior of protons, electrons, and alpha particles across the interface suggests that it separates plasma of different origins; ii) there is a strong shear flow at the interface; iii) the magnetic field strength maximizes near the interface and is roughly constant across it; and iv) although their observations were made during the descending phase of Solar Cycle 20, the interfaces did not generally recur from one solar rotation to the next.

Recently, Riley *et al.* (2012b), studied two specific properties of CIRs: the orientation of the SIs during the solar cycle minimum and the occurrence rate of both F and R CIR shocks near the ecliptic plane through Solar Cycle 23. They employed a global magnetohydrodynamic (MHD) model to understand the observations. The model reveals the complex evolution of CIRs at different heliographic latitudes and longitudes. CIR properties (*i.e.*, orientations) depend on location and size of the coronal holes associated with the fast SW. In particular, in the vicinity of the solar minimum, the CIRs present clear latitudinal tilts at mid-heliolatitudes but no systematic tilts around the ecliptic plane. On the other hand, in general, the ratio of F to R shocks observations near the ecliptic plane at 1 AU is greater than one and varies along the solar cycle. The global model shows that because CIR dynamics are not centered in the ecliptic, but at latitudes where there are longitudinal gradients in speed back at the Sun, in-ecliptic spacecraft tend to intercept the CIR structures at their flanks. Thus, except in the case of equatorial coronal holes producing CIRs centered around the equator, F shocks tend to penetrate to lower latitudes than R shocks. This explains why it is more likely to detect F shocks than R shocks near the ecliptic plane.

In this study, we analyze multi-spacecraft in-ecliptic observations of CIRs during the ascending phase of the Solar Cycle 21 employing an unique data set. Reanalyzing these

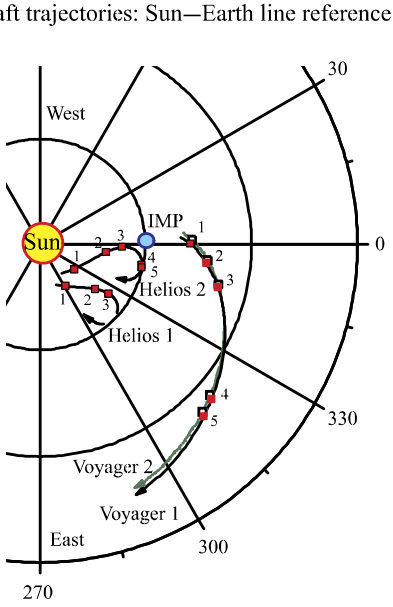

Figure 1 Trajectories of the five spacecraft from November 1977 to March 1978 as observed in a reference system with the Sun–Earth line fixed. The squares denote the spacecraft positions at the five CIR events (solid squares are V1 measurements and open squares V2 measurements). The blue dot is the Earth at 1 AU.

data contributes to our understanding of the three-dimensional geometry and evolution of the solar wind dynamics during the ascending phase of the cycle. The outline of the paper is as follows: in Section 2 we show the five spacecraft trajectories, the patterns of SW streams (bulk speed and total pressure) detected by the spacecraft, and we identify five CIR events; in Section 3 we discuss CIR properties and geometries; in Section 4 we discuss the SW streams predicted by the global MHD model and its relation with the CIR geometry, and, finally, in Section 5 we present our conclusions.

2. Five-Spacecraft Simultaneous Observations

We obtained trajectory files and one-hourly averaged SW plasma and magnetic field data from the five spacecraft from the Coordinated Heliospheric Observations (COHO) Web at the National Space Science Data Center (NSSDC) (http://nssdc.gsfc.nasa.gov/cohoweb/cw.html). Figure 1 shows the five spacecraft trajectories from a corotating reference system where the Sun–Earth line is fixed. In this frame IMP is always located at 1 AU along the Sun–Earth line (blue dot), while the other four spacecraft are continuously changing positions. The *Helios* remained within the inner heliosphere covering a heliocentric range from 0.3 to 1.0 AU, whereas, during this interval, the *Voyagers* were on their way to Jupiter covering a heliocentric range from 1.2 to 2.5 AU. In November 1977, *Helios 1* was located eastward with respect to the other four spacecraft, but by March 1978 the *Voyagers* were the ones eastward with respect to the other spacecraft.

When we compare the observations of a particular event by several spacecraft at different locations, we note that the event occurs at different times in each spacecraft data series and we need to infer their positions with respect to the event. In our case the reference system in Figure 1 corotates with the Earth with an angular speed of about $360°/365$ days, $\sim 0.99°$ per day, and it is necessary to consider this displacement when we combine the observations of different spacecraft at different times. On the other hand, the source of SW streams (*i.e.*, the

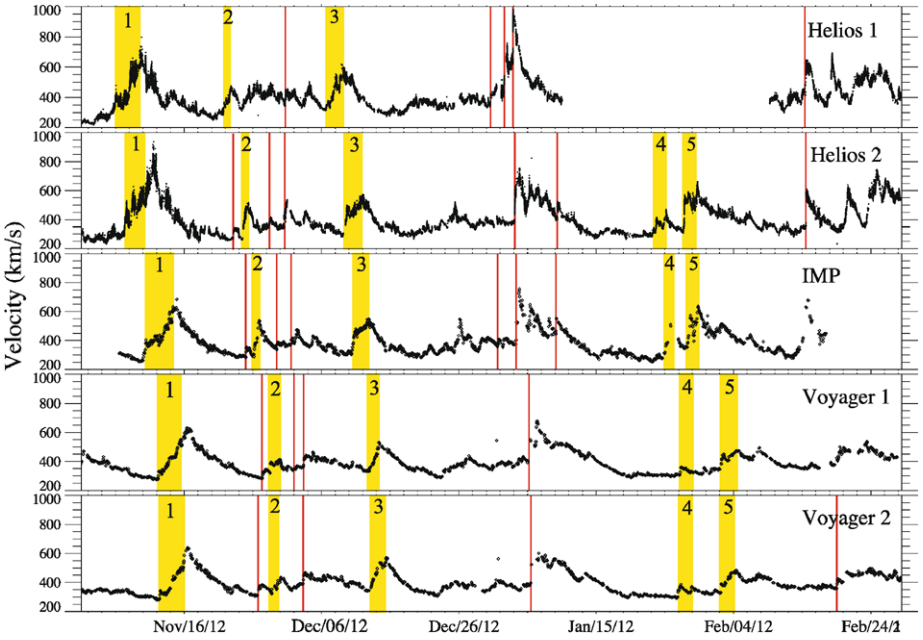

Figure 2 Solar wind speed measurements from the five spacecraft from November 1977 to March 1978. The solid yellow boxes indicate the five CIR events, whereas the vertical lines indicate transient forward shocks. The data were obtained from the COHO-Web at the NSSDC.

solar surface) has an equatorial angular speed of about 360°/25 days, ∼ 14.4° per day, in addition to the angular displacement of the spacecraft itself. This implies that the spacecraft SW data series is associated with a succession of different regions on the solar surface. Finally, a further complexity in this analysis is that the solar atmosphere is not just rotating but continually changing, in particular during the ascending phase and solar maximum.

2.1. Identification of Solar Wind Structures

During the ascending phase of the solar cycle the SW permeating the IP medium near the ecliptic plane is characterized by a highly varying slow SW with transient forward shocks and coronal mass ejections (CMEs); there are also weak CIRs caused by 'thin' and not very fast SW streams ($\sim 500-600$ km s^{-1}), which, in general, have different geometries and radial widths than those CIRs produced in the descending phase of the cycle. Figure 2 shows the plots of radial SW speed, V_r, measured simultaneously by the five spacecraft from November 1977 to March 1978. Although the angular separations of the spacecraft were changing continuously in this interval, we can recognize the same patterns of V_r in the five plots. Figure 2 indicates the CIR events and transient forward shocks identified in the five data sets. The bulk speed is the most stable SW parameter and the plots show that this is true for a range of longitudes. There is a modest corotating fast stream ($\sim 500-600$ km s^{-1}) appearing about every 27 days causing CIRs (events 1, 3, and possibly 5 in Figure 2). This recurrent fast stream is coexisting with an unstable ambient slow SW and transient events. In some regions this slow SW is very slow indeed (~ 220 km s^{-1}). Note the 'filtering' of SW speeds with heliocentric distance, the speed difference between slow and fast SW is higher in H1 and H2 measurements than in V1 and V2 observations.

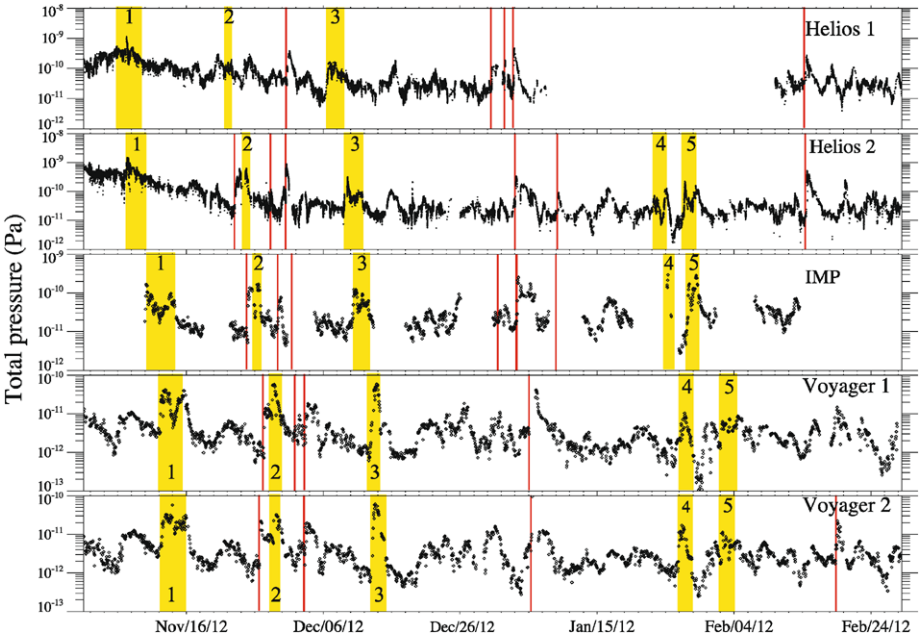

Figure 3 Solar wind total pressure measurements of the five spacecraft from November 1977 to March 1978. The solid boxes indicate the five CIR events, whereas the vertical lines indicate transient forward shocks. The data were obtained from the COHO-Web at the NSSDC.

Figure 3 shows the total pressure (P_t) as measured by the five spacecraft. This physical parameter is also very helpful to recognize the same event in the five data sets; it reveals the presence of large-scale compressive structures which, combined with the bulk speeds in the previous figure, clearly show the shock events associated with CIRs and CMEs. Figure 3 indicates the CIR events and transient forward shocks identified in the data sets.

On the other hand, the *in-situ* measurements of proton density (N_p), proton temperature (T_p), and magnetic field magnitude ($|\mathbf{B}|$) present very different signatures between the five data sets, so they are not as helpful in identifying the coinciding IP events. The properties of the ambient SW in this period were very unstable. The local variations in N_p, T_p, and $|\mathbf{B}|$ measurements reveal the presence of many local structures. These inhomogeneities affect the wave fronts propagating through the IP medium and deform the shape of the large-scale SW events.

With the data obtained from the COHO Web we produced a series of 27-day plots of V_r, N_p, T_p, P_t, and $|\mathbf{B}|$ for each spacecraft. We visually inspected the 27-day plots looking for the characteristic CIR signatures as described by González-Esparza *et al.* (1996). We found five CIRs in this four month interval. We corroborated the shock identifications by plotting each shock in detail in high time resolution data from the experiments' web pages and check them against the H1–H2 shock list by Volkmer and Neubauer (1985), the IMP shock list by Borrini *et al.* (1982) and the V1–V2 studies by Gazis and Lazarus (1983), Burlaga *et al.* (1984), and González-Esparza and Smith (1996). Table 1 presents spacecraft positions and times for the five events and some properties that we will discuss in the next sections. In Figures 1, 2, and 3, the CIRs are indicated by their numbers (1 to 5).

Table 1 List of CIR events: spacecraft identification, Earth–Sun–spacecraft (ESS) angle, spacecraft heliocentric distance, CIR initial time, CIR radial width (Δ_{cir}), location of the stream interface with respect to the normalized CIR radial width (δ_{si}), speed of the upstream fast wind, speed of the upstream slow wind, ratio of dynamic pressures between fast and slow winds, and presence of F and/or R shocks bounding the CIR. (*) indicates a data gap at some part of the event which affects the estimation of the parameter, n/s indicates that no shock was observed.

Id.	ESS (°)	R_d (AU)	Time (d:m:hr)	Δ_{cir} (AU)	δ_{si}	Fast SW (km s^{-1})	Slow SW (km s^{-1})	P_f/P_s	Shock (F/R)
CIR 1									
H1	303	0.47	07-November-18	0.30	n/si	563 ± 55	390 ± 28	0.5	F
H2	326	0.40	07-November-19	0.23	0.21	480 ± 9	296 ± 8	0.67	F
IMP	0	1.0	10-November-13	0.21*	0.19*	396 ± 11	262 ± 8	1.07	n/s
V1	0	1.43	12-November-18	0.39	0.21	575 ± 17	281 ± 4	2.83	F
V2	2	1.45	12-November-23	0.36	0.26	577 ± 28	288 ± 5	2.28	F
CIR 2									
H1	322	0.69	24-November-20	0.27	0.69	390 ± 2	319 ± 5	1.38	n/s
H2	354	0.63	25-November-02	0.24*	0.22*	460 ± 17	266 ± 6	1.02	gap
IMP	0	1.0	26-November-17	0.19*	0.21*	488 ± 51	303 ± 5	0.5	gap
V1	354	1.58	29-November-02	0.28	0.41	403 ± 8	324 ± 4	0.59	F
V2	354	1.59	29-November-07	0.28	0.45	425 ± 6	323 ± 4	1.21	F
CIR 3									
H1	324	0.79	07-December-03	0.11	0.44	350 ± 15	319 ± 4	0.9	n/s
H2	358	0.77	09-December-08	0.24	0.53	473 ± 11	309 ± 4	1.9	n/s
IMP	0	1.0	10-December-16	0.18	0.51	490 ± 11	315 ± 5	1.6	n/s
V1	346	1.73	13-December-11	0.31	0.58	528 ± 5	334 ± 2	1.4	R
V2	347	1.74	13-December-16	0.24*	0.29*	515 ± 5	349 ± 5	1.8	gap
CIR 4									
H1	*	data gap							
H2	349	0.98	23-January-15	0.18	0.60	379 ± 5	292 ± 5	1.54	n/s
IMP	*	data gap							
V1	317	2.19	27-January-19	0.26*	0.33*	321 ± 4*	301 ± 3*	0.86*	gap
V2	318	2.15	27-January-10	0.25	0.41	341 ± 4	302 ± 4	0.76*	F
CIR 5									
H1	*	data gap							
H2	347	0.98	28-January-05	0.20	0.15	613 ± 12	312 ± 2	1.19	n/s
IMP	0	1.0	28-January-19	0.17	0.23	607 ± 8	353 ± 4	0.87	n/s
V1	314	2.25	02-February-17	0.24	0.39	407 ± 7	352 ± 4	1.62	F
V2	314	2.21	02-February-17	0.24	0.52	427 ± 8	350 ± 6	1.11	F

2.2. Maps of Large-Scale Features

In this section we summarize and unify the observations of dynamic structures detected by the five spacecraft using the maps of large-scale structures. These maps use the format of 27-day rows to approximate the equatorial solar rotational period, as observed by the spacecraft, integrating the events using different data sets. Figure 4 shows the maps of the five spacecraft, the rows are ordered chronologically from bottom to top. In the central right panel we show the symbols representing the structures. The interplanetary magnetic field (IMF)

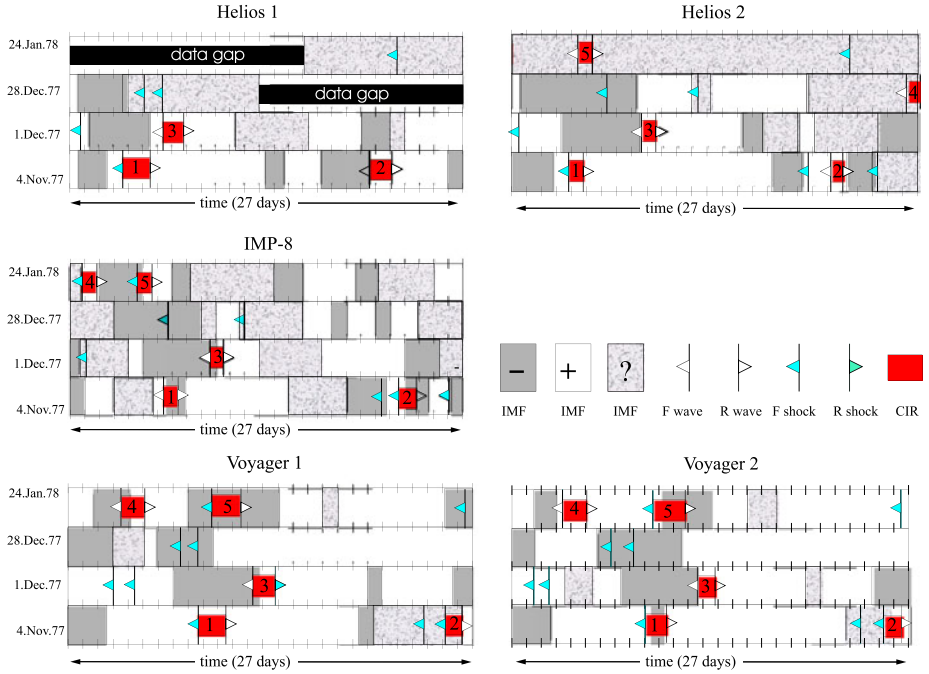

Figure 4 Maps of large-scale solar wind features detected by the five spacecraft. Every 27-day row corresponds to an approximate solar rotation observed by the spacecraft. The chronological order is from bottom to top. The central right panel indicates the symbol codes (see also the text).

polarity is shown as the background of the 27-day row, it can be either positive (white), negative (gray), or of undetermined sign if its orientation is very unstable or there is a data gap (stippled gray). A heliospheric current sheet (HCS) crossing is indicated by a discontinuous change of IMF polarity. IP shocks are represented by blue arrows, F shocks pointing to the left, and R shocks to the right. Compressive waves (*i.e.*, no shock waves) are represented by open arrows. CIRs are denoted by red boxes and are identified by their numbers (Table 1). By definition, CIR shocks appear bounding CIRs, whereas transient shocks are unrelated to CIRs. We can expect that, in general, the CIRs are bounded by shocks beyond 1 AU; but in many cases these shocks might have not yet formed, or there are geometrical effects involved, and these CIRs appear bounded only by compressive waves.

2.3. Magnetic Sectors

The IMF polarity is a useful signature to trace back the origin of SW streams. This is the idea of representing the IMF polarity in the maps of large-scale features, it also points out the HCS crossings. Note that *Helios* and *Voyager* IMF data are in the Radial Tangential Normal (RTN) coordinate system (R is positive when pointing away from the Sun), whereas IMP IMF data are in the Geocentric Solar Ecliptic (GSE) coordinate system (in this case x_{GSE}, which corresponds to R, is positive when pointing towards the Sun). We considered this fact to infer the IMF polarity. If the corotating SW sources were stable, we would have expected that the magnetic polarities in the five maps in Figure 4 were very similar, perhaps only with some differences attributed to the evolution with radial distance and the changing

spacecraft longitudes. However, in general, the extension and location of the magnetic sectors in each map do not corotate with the 27-day period and suggest an unstable behavior. We find local variations when comparing the IMF polarity observations. These fluctuations in the magnetic sector measurements by the *Helios*, IMP, and the *Voyagers* imply a complicated evolution with heliocentric distance, where the HCS becomes warped with local fluctuations. The maps in Figure 4 indicate several CIRs embracing the HCS crossings. In many cases, fast SW streams overtake slow SW streams associated with the HCS. In this interaction we find not only two different SW streams, but different magnetic polarities.

3. CIR Analysis

Now we discuss some characteristics of the five events based on Figures 1, 2, 3, and 4 and Table 1.

CIR 1. This event was associated with the widest fast SW stream detected during this study, which reappeared, 27 days after, in the following solar rotation (Figure 2). In all the spacecraft the fast SW carries a positive IMF, except at IMP (Figure 4). This negative IMF fast SW lasts only for about one day. In H1, H2, V1, and V2 measurements, the CIR was bounded by a F shock, but there was no shock at IMP. Note that in this case, the Earth was located westward from H1, H2, V1, and V2, which might explain the difference with IMP data. The ratio of dynamic pressures between fast and slow SWs were lower than one in *Helios* data, and higher than one in the *Voyager* data.

CIR 2. This CIR was analyzed previously by Burlaga *et al.* (1980). This is a weak stream interaction (Figure 2), where H2 and IMP were aligned, and H1, V1, and V2 were eastward from Earth. At H1, V1, and V2, the fast SW associated with the CIR carries a positive IMF, but at IMP and H2 the polarity is negative (Figure 4). This fast SW stream was weak and disappeared in the next solar rotation. There were F shocks at V1 and V2.

CIR 3. This event detected by the five spacecraft is very likely associated with the reappearance of the fast stream causing CIR 1. The fast SW carried positive magnetic field in all the spacecraft and the CIR included a HCS crossing. The interaction region was very weak, and, in fact, there were no F shocks in the five spacecraft (Figure 4). This was the only event with a R shock at V1 location, whereas there was a data gap at V2.

CIR 4. The event showed a speed profile similar to CIR 2, resembling a transient fast SW (Figure 2) causing a weak interaction region. The streams associated with this CIR were very slow indeed; the slow SW was about 292 – 302 km s^{-1} and the fast SW was only about 321 – 379 km s^{-1}. There was only an F shock at V2. Note that the fast SW carried positive magnetic field at V1, V2, and IMP (Figure 4, there was data gap at H1 and we could not determine the IMF polarity at H2).

CIR 5. The CIR was detected by four spacecraft (data gap in H1). It was produced by fast SW with negative IMF polarity at V1 and V2, but with positive at IMP (we could not determine the IMF polarity at H2). Although the fast streams were significantly slower at V1 and V2, as compared with H2 and IMP observations, we only found F shocks at V1 and V2. This disparity with the IMF polarity in IMP data is puzzling, a latitudinal effect seems possible.

3.1. Geometry of Stream Interfaces

Figure 5 shows the relative position (rp) of the SIs with respect to the CIR radial width normalized to 1. This parameter indicates whether the SI was located closer to the front

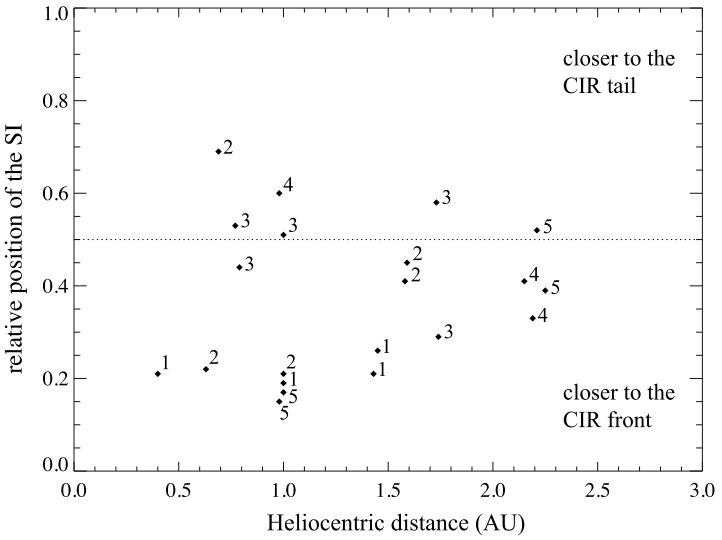

Figure 5 Relative position of the stream interfaces (SIs) with respect to the CIRs. The radial width of the CIR is normalized to 1. The numbers indicate the CIR event.

($0 < \mathrm{rp} < 0.5$), trailing edge ($0.5 < \mathrm{rp} \leq 1.0$) or in the middle of the CIR ($\mathrm{rp} = 0.5$), with respect to the in-ecliptic radial cut by the spacecraft. This SI location, in terms of the CIR boundaries, depends on the CIR characteristics, geometry (latitudinal inclination), and its heliocentric evolution. Fifteen out of the 21 SIs analyzed in this study were located closer to the forward boundary ($0 < \mathrm{rp} < 0.5$). This result must be related to the fact that most of the CIRs were bounded by F shocks and R compressive waves (no shocks at the trailing boundary). There was only one event (CIR 3) having $\mathrm{rp} > 0.5$ in most of the spacecraft, this was also the only CIR bounded by a R shock. This event included a swept up HCS crossing within the interaction region. Note that Figure 5 suggests a tendency where the data points approach to the middle of the CIR ($\mathrm{rp} = 0.5$) as the heliocentric distance increases. However, we would require more data points at farther distances to assess whether this is a real effect related with the CIR heliocentric evolution.

Table 2 shows the latitudinal inclinations and average radial speeds of the SIs detected by the five spacecraft. In order to infer the SI orientation we applied the technique described by González-Esparza and Smith (1997), which basically relies on analyzing velocity data around the SI to determine the normal direction to the SI plane. We applied the minimum variance analysis to the velocity components (taking about one-hour averages upstream and downstream of the SI using high time resolution data). The idea is to determine the minimum (null component) and maximum variance directions, both contained within the SI plane, and the intermediate variance direction, normal to the SI plane. The velocity components are then rotated to this new system of reference. We then determined the SI latitudinal inclination with respect to the ecliptic plane using the direction normal to the SI plane. We report the standard deviation of the radial velocity in Table 2 to provide an estimate of its variability around the SI plane. It should be kept in mind that, as happens with other techniques using *in-situ* measurements to analyze MHD discontinuities, the solutions were very sensitive to the arbitrary selection of the upstream and downstream intervals. However, we performed several tests to check the stability of the solutions confirming the sign and magnitude of the inclinations. The SI orientations of CIRs 1, 3, and 5, all showed positive

Table 2 Analysis of the stream interface (SI) orientations: CIR number, spacecraft, SI latitudinal declination, and SI mean radial speed. (∗) indicates a data gap around the stream interface.

CIR no.	Spacecraft id.	SI dec. (°)	$\langle V_{si} \rangle$ (km s^{-1})
1	H1	18.5	450±68
	H2	27.5	434±16
	IMP	37.5	351±16
	V1	38.2	349±14
	V2	25.9	323±4
2	H1	−24.8	391±9
	H2	−27.6	425±20
	IMP	−10.3	434±17
	V1	29.0	384±4
	V2	12.0	367±3
3	H1	*	363±5
	H2	14.1	404±8
	IMP	11.0	394±15
	V1	7.6	396±7
	V2	n/s	420±8
4	H1	*	gap
	H2	−30.7	379±26
	IMP	*	gap
	V1	−16.3	349±4
	V2	−25.1	369±8
5	H1	*	gap
	H2	37.6	507±61
	IMP	*	gap
	V1	36.1	443±9
	V2	*	gap

inclinations, indicating that their fronts were pointing towards the ecliptic plane and their tails were pointing northwards. On the other hand, CIRs 2 and 4 presented SIs with negative inclinations. In these later cases, their fronts were pointing towards the ecliptic plane and their tails faced southward.

It is interesting to compare the results in Table 2, the solar wind streams in Figure 2, and the large-scale maps of Figure 4. CIRs 1 and 3 originated with a corotating fast SW stream reappearing around 27 days later (Figure 2). The fast stream had positive magnetic polarity (Figure 4) and was coming from a northern coronal hole. All the SIs associated with these events presented positive SI inclinations (Table 2). On the other hand, CIRs 2 and 4 were associated with weaker fast SW streams (Figure 2), disparate magnetic polarities (Figure 4), and mixed SI inclinations (dominated by negative values, Table 2).

3.2. Ratio of Solar Wind Dynamic Pressures

Figure 6 shows the ratio of dynamic pressures between the fast and slow SW associated with the CIRs. This parameter indicates whether the fast wind transfers momentum to the slow wind ahead (acceleration of the slow SW), or the opposite (deceleration of the fast SW). In most of the events (14/8) the ratio was larger than one, indicating that the fast stream had

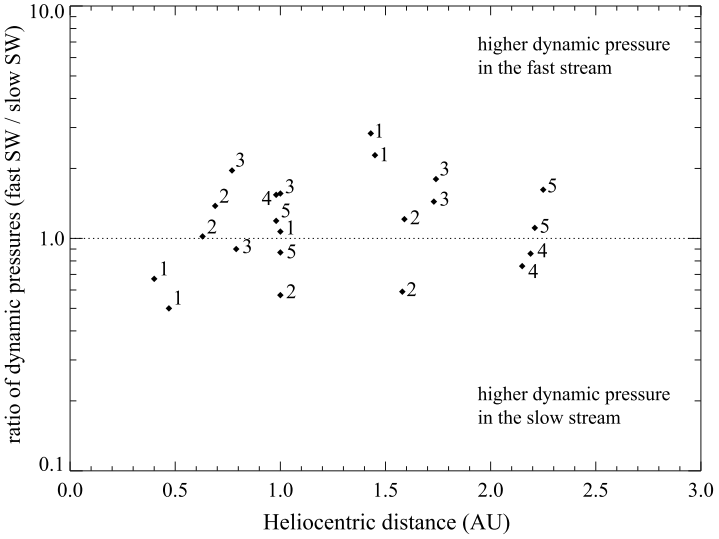

Figure 6 Ratio of dynamic pressures between the fast and slow SW associated with the CIRs as detected by the five spacecraft. The numbers indicate the CIR event.

more dynamic pressure, so the momentum was flowing from the fast SW to the slow SW (outward from the Sun). However, there were also several cases where the ratio was lower than one, indicating that the momentum was flowing sunward. It is interesting to note that there were events (*i.e.*, CIRs 1 and 2) where different spacecraft detected opposite ratios. This also indicates significant inhomogeneities in the solar wind streams, which affect the shape and evolution of CIR events.

4. Global MHD Model

In this section, we employ a global magneto-hydrodynamic (MHD) model of the solar corona and inner heliosphere to interpret some properties of the CIR *in-situ* measurements presented in previous sections. The modeling technique is described by Riley, Linker, and Mikic (2001). The model solves the full set of resistive MHD equations and uses photospheric synoptic magnetograms as initial conditions, which allows us to compute solutions for specific times (whenever the magnetic data are available). The numerical simulations employ an empirical coupling between the coronal and heliospheric models and, in the absence of obvious transient activity, the solar wind streams solutions given by the model do match observations reasonably well.

We applied the global MHD model to analyze the time interval studied in this paper (CR 1661 – 1664). Unfortunately, there was no magnetogram available for CR 1661 and 1663. On the other hand, since we were in the ascending phase of the cycle, there were some times with significant transient activity.

Following Riley *et al.* (2012a), Figure 7 shows the solutions of the global MHD model at 1 AU for Carrington rotation 1662. The pressure profile (left panel) indicates the sections where we would expect compression regions associated with the SW stream dynamics, whereas the latitudinal velocity profile (right panel) indicates the shear flows associated

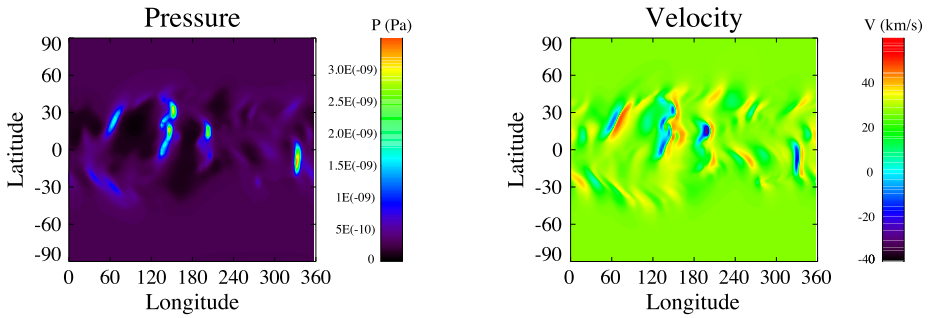

Figure 7 Global profiles at 1 AU for Carrington rotation 1662 obtained from the global MHD model: (left) thermal pressures and (right) latitudinal velocities.

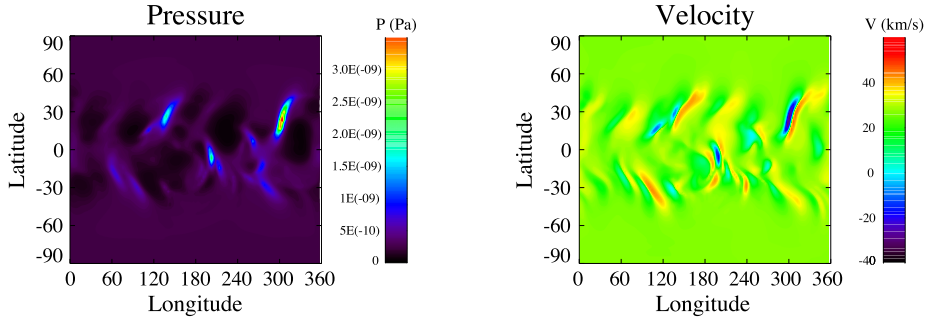

Figure 8 Global profiles at 1 AU for Carrington rotation 1664 obtained from the global MHD model: (left) thermal pressures and (right) latitudinal velocities.

with the orientation of these sections. This orientation is related to the latitudinal inclination of the CIRs. The pressure profiles show a compressional structure at around 130° longitude crossing the ecliptic plane, which was associated with a northern mid-latitude coronal hole. The structure presented a small latitudinal tilt and was surrounded by two rarefaction regions (dark areas). This equatorial "streak" had its front pointing towards the ecliptic plane, whereas its trailing lobe pointed towards northern latitudes. This compressional feature is associated with CIR 3, which presented a similar orientation (Table 2). The latitudinal velocities (Figure 7, right panel) indicate that shear flows (red and blue areas) were associated with this compression structure. In this case we found a good qualitative agreement between the CIR observation and the numerical results given by the global MHD model.

Figure 8 shows the solutions of the global MHD model at 1 AU for CR 1664. We note significant changes with respect to the previous figure, showing the varying conditions associated with the ascending phase of the solar cycle. There were not large compression features crossing the ecliptic plane. CIR 4 was associated with the weakest fast SW stream in this analysis (Table 1), so this might explain why a clear counterpart did not appear in the pressure profile. On the other hand, we find a similar problem for CIR 5, but its counterpart could be the compression feature at around 310° longitude, which presented about the same inclination as the *in-situ* measurements (Table 2).

5. Summary and Conclusions

We presented a study of simultaneous *in-situ* multi-spacecraft observations of CIRs during the ascending phase of Solar Cycle 21. The conjunction of the five spacecraft makes this interval unique for the purposes of studying the dynamics of the IP medium; in particular, the data set sheds light on several aspects of the geometry and heliocentric evolution of the CIRs. In order to integrate the five-spacecraft observations, we examined the patterns of SW streams (bulk speed, total pressure, entropy, proton density, temperature, and magnetic field magnitude and direction), identifying five CIR events, and produced maps of IP large-scale features, unifying and summarizing the data. These maps indicate the large-scale compressive events and the magnetic sectors associated with the SW streams causing the CIRs. The maps show those events to be associated with HCS crossings.

The CIRs were associated with weak fast streams coming from mid latitude coronal holes. We did not find strong stream interactions associated with large polar coronal holes (characteristic of the descending phase or solar minimum). Most of the CIR events were lead by an F shock and trailed by a compressive wave. In fact, there was only one R shock case in the five spacecraft data set.

As expected, most of the CIRs detected by H1 and H2 were bounded by compressive waves; whereas the F shocks were more likely detected by IMP, V1, and V2. The frequency of F shocks leading CIRs increased with the heliocentric distance.

In general, as expected, we found the same IMF polarity in the five measurements of the fast SW stream causing a particular CIR; however, there were two cases (CIRs 1 and 5) with an inconsistency (different polarities) in IMP observations.

We analyzed the distribution of the relative position of the SIs embedded within the CIRs. This parameter is related to the dynamics and geometry between fast and slow streams associated with the CIR. More than 70 % of the SIs in this study were located closer to the forward edge. This result must be associated with the fact that most of the CIRs were bounded by F shocks only. On the other hand, the data suggest a tendency of the data points to approach to the center of the CIR (rp $= 0.5$) as the heliocentric distance increases. However, this result requires more observations to determine if this is a real effect related to the CIR heliocentric evolution.

From the analysis of the geometry of the SIs, we found that all the CIRs presented latitudinal tilts with respect to the ecliptic plane. This result is in agreement with the origin of the fast streams coming from mid-latitude coronal holes and the predominance of F shocks over R shocks bounding the CIRs.

The distribution of the ratio of dynamic pressures between fast and slow SW streams related to the CIR events, indicate that in about 60 % cases the fast stream transferred momentum to the slow one ahead; but in about 40 % of cases the ratio was lower than one, indicating that the momentum was flowing sunward. The variability of this parameter points out significant inhomogeneities in the SW streams. This irregularity in the direction of the momentum flow should affect the shape, geometry, and heliocentric evolution of CIRs, causing local deformations in the inner heliosphere. However, we expect that at farther heliocentric distances, since the SW density decreases with the square of the distance, the dynamic pressure of the fast stream becomes dominant while these local inhomogeneities become less important.

The global MHD model shows that, during the ascending phase of the solar cycle, the CIR dynamics are not centered in the ecliptic, but at latitudes where there are longitudinal gradients in speed back at the Sun, thus in-ecliptic spacecraft tend to intercept the CIR structures at their flanks. Therefore, except in the case of equatorial coronal holes producing

CIRs centered around the equator, the F shocks tend to penetrate to lower latitudes than R shocks. This explains why it is more likely to detect F shocks than R shocks near the ecliptic plane in the ascending phase of the cycle. The comparison between the observations and the model gave mixed results. In general, there was a qualitative agreement between the geometry of the pressure features at 1 AU predicted by the global model and the inclination of the SIs obtained from *in-situ* data. However, this comparison was limited because there were not enough magnetic data for two CRs (1662, 1664), besides that there were some periods of high transient activity, which cannot be handled by the model.

The results of this study show some interesting aspects of the CIR dynamics related to the relative position of the stream interface or to the ratio of dynamic pressures, which deserve a further study to cover larger heliocentric ranges. The dispersion of the data points does not allow us to find clear tendencies for these parameters with the heliocentric distance, but presumably at farther distances, where the CIRs become stronger and wider, the local fluctuations should decrease and the global properties become dominant. We would expect then clearer tendencies.

Acknowledgements We thank the referee for the useful comments. This project was partially supported by DGAPA PAPIIT IN105310-3 and CONACyT 152471 projects. E. Romero-Hernandez thank to CONACyT for her Ph.D. grant. The plasma and magnetic field data for this study were obtained from the National Space Science Data Center at Goddard Space Flight Center. We also thank the principal investigators: Prof. J.W. Belcher (plasma experiment V1 and V2), Dr. N.F. Ness (magnetometers H1, H2, V1 and V2), Dr. H.R. Rosenbauer (plasma experiment H1 and H2), Dr. R.P. Lepping (magnetometer IMP-8) and Dr. A. Lazarus (plasma experiment IMP-8).

References

Balogh, A., Gonzalez-Esparza, J.A., Forsyth, R.J., Burton, M.E., Goldstein, B.E., Smith, E.J., Bame, S.J.: 1995, Interplanetary shock waves: Ulysses observations in and out of the ecliptic plane. *Space Sci. Rev.* **72**, 171.

Borrini, G., Gosling, J.T., Bame, S.J., Feldman, W.C.: 1982, An analysis of shock wave disturbances observed at 1 AU from 1971 through 1978. *J. Geophys. Res.* **87**, 4365.

Burlaga, L.F.: 1974, Interplanetary stream interfaces. *J. Geophys. Res.* **79**, 717.

Burlaga, L., Goodrich, C., Sullivan, J., Gurnett, D., Kellogg, P., Keppler, E., Mariani, F.: 1980, Interplanetary particles and fields, November 22 to December 6, 1977 – Helios, Voyager and IMP observations between 0.6 and 1.6 AU. *J. Geophys. Res.* **85**, 2227.

Burlaga, L.F., Lepping, R.P., Behannon, K.W., Klein, L.W.: 1984, Large-scale interplanetary magnetic fields – Voyager 1 and 2 observations between 1 AU and 9.5 AU. *J. Geophys. Res.* **89**, 10659.

Gazis, P.R., Lazarus, A.J.: 1983, The radial evolution of the solar wind, 1 – 10 AU. In: Wilcox, J.M., Hundhausen, A.J. (eds.) *Solar Wind Five* **228**, 509.

González-Esparza, J.A.: 1999, Geometry and radial width of interaction regions. In: Habbal, S.R., Halas, C.D. (eds.) *The Solar Wind Nine Conference*, *AIP Conf. Proc.* **471**, 593.

González-Esparza, J.A., Smith, E.J.: 1996, Solar cycle dependence of the solar wind dynamics: Pioneer, Voyager, and Ulysses from 1 to 5 AU. *J. Geophys. Res.* **101**, 24359.

González-Esparza, J.A., Smith, E.J.: 1997, Three-dimensional nature of interaction regions: Pioneer, Voyager, and Ulysses solar cycle variations from 1 to 5 AU. *J. Geophys. Res.* **102**, 9781.

González-Esparza, J.A., Balogh, A., Forsyth, R.J., Neugebauer, M., Smith, E.J., Phillips, J.L.: 1996, Interplanetary shock waves and large-scale structures: Ulysses' observations in and out of the ecliptic plane. *J. Geophys. Res.* **101**, 24359.

Gosling, J.T., Asbridge, J.R., Bame, S.J., Feldman, W.C.: 1978, Solar wind stream interfaces. *J. Geophys. Res.* **83**, 1401.

Gosling, J.T., Bame, S.J., McComas, D.J., Phillips, J.L., Pizzo, V.J., Goldstein, B.E., Neugebauer, M.: 1993, Latitudinal variation of solar wind corotating stream interaction regions: Ulysses. *Geophys. Res. Lett.* **20**, 2789.

Pizzo, V.J.: 1991, The evolution of corotating stream fronts near the ecliptic plane in the inner solar system. II – Three-dimensional tilted-dipole fronts. *J. Geophys. Res.* **96**, 5405.

Pizzo, V.J., Gosling, J.T.: 1994, 3-D simulation of high-latitude interaction regions: comparison with Ulysses results. *Geophys. Res. Lett.* **21**, 2063.

Riley, P., Linker, J.A., Mikic, Z.: 2001, An empirically-driven global MHD model of the solar corona and inner heliosphere. *J. Geophys. Res.* **106**, 15889.

Riley, P., Gosling, J.T., Weiss, L.A., Pizzo, V.J.: 1996, The tilts of corotating interaction regions at midheliographic latitudes. *J. Geophys. Res.* **101**, 24349.

Riley, P., Linker, J.A., Lionello, R., Mikic, Z.: 2012a, Corotating interaction regions during the recent solar minimum: the power and limitations of global MHD modeling. *J. Atmos. Solar-Terr. Phys.* **83**, 1.

Riley, P., Linker, J.A., Gonzalez-Esparza, J.A., Jian, L., Russell, C.T., Luhmann, J.G.: 2012b, Interpreting some properties of CIRs and their associated shocks during the last two solar minima using global MHD simulations. *J. Atmos. Solar-Terr. Phys.* **83**, 11.

Siscoe, G.L.: 1976, Three-dimensional aspects of interplanetary shock waves. *J. Geophys. Res.* **81**(34), 6235.

Siscoe, G.L., Finley, L.T.: 1969, Meridional (North–South) motions of the solar wind. *Solar Phys.* **9**, 452. doi:10.1007/BF02391671.

Volkmer, P.M., Neubauer, F.M.: 1985, Statistical properties of fast magnetoacoustic shock waves in the solar wind between 0.3 AU and 1 AU – Helios-1, 2 observations. *Ann. Geophys.* **3**, 1.